DENSITY DEPENDENT NUCLEON–NUCLEUS OPTICAL POTENTIAL IN THE (p, n) REACTIONS

Ahmed Osman

Physics Department, Faculty of Science, Cairo University, Cairo, Egypt

(Received December 1, 2008; revised version received May 5, 2009)

The quasielastic (p, n) reactions are studied for different incident proton energies. Transitions to isobaric analog states are obtained for different target nuclei with masses $13 \leq A \leq 208$. The nucleon–nucleus interactions are considered to be density dependent in the optical model potential. Microscopic and macroscopic distorted-wave Born approximation (DWBA) calculations with the optical model potential are introduced. Differential cross-sections and angular distributions are calculated for different (p, n) reactions. The present theoretical calculations are in good agreement with the experimental data.

PACS numbers: 24.10.Ht, 25.40.Kv, 25.40.Cm, 25.40.Dn

1. Introduction

Heavy ion scattering [1] and the scattering of nucleons from nuclei [2] have been widely considered in the last few years. The nucleon–nucleon effective interactions describing the target nuclei are taken density-dependent from realistic free nucleon–nucleon forces. The mass operator is calculated from the hard core free nucleon–nucleon interaction and introduced on energy shell to the optical model potential to be applied to finite nuclei through the improved local density approximation. The energy variations of the potential depth of the optical model potential are parametrized to reproduce the proton scattering and the reaction for spherical and soft nuclei [2] and deformed stable and unstable isotopes [3]. Calculations of the symmetric and asymmetric terms of the optical model potential show [4] that the isovector components are very weak. Energy-dependent nucleon–nucleus potential depth are parametrized and compared with nucleon elastic and quasielastic scattering observables to separate isoscalar and isovector optical potential components, using finite-range density-dependent forces.

Isobaric analog states are shown [5] as useful source for understanding nuclear structure of nuclei, and explaining [6] the charge-independence- and charge-symmetry-breaking interactions [7] in nuclei. The isobaric analog states introduce [8] helpful study showing the relation between the giant isovector monopole state and the isovector part of the nucleon–nucleus potential. The isovector nucleon–nucleus potential can be extracted from the optical model describing the transitions in the (p,n) reactions for which the total angular momentum and parity transferred are 0^+, known as quisielastic scattering. Extending the analyses for wide range of target nuclei and wide range of incident energies, the imaginary strength of the optical potential were found [9] independent of the mass number. The obtained parameters of the isovector potential are found as A-dependent parameters of the potential.

In the present work, the quasielastic scattering (p,n) reactions are considered. The (p,n) reactions are studied for a wide range of target nuclei and for different values of the incident energies. Optical model potential are used to explain these reactions for each target nucleus. The isovector term of the nucleon–nucleus potential is extracted for each case. Nucleon–nucleon effective interaction is constructed as finite range, density dependent effective interaction from realistic free nucleon–nucleon forces. The optical model analyses of the isobaric analog states transitions are introduced in the (p,n) reactions. Differential cross-sections of the quasielastic (p,n) reactions are calculated for different incident proton $E_p = 23$ MeV, 26 MeV and 35 MeV incident on the different target nuclei ^{13}C, ^{70}Zn, ^{96}Zr, ^{112}Sn, ^{124}Sn and ^{208}Pb. Numerical calculations are carried out for the angular distributions of the (p,n) reactions leading to isobaric analog states. The systematic optical model analyses, and the result of calculated angular distributions are compared with the experimental data.

In Section 2, we introduce the formulation of the optical model potential and the distorted wave Born approximation. Numerical calculations and results are given in Section 3. Section 4 is left for discussion and conclusions.

2. Optical model potential and DWBA

The nucleon–nucleus optical model potential including isospin symmetry in nuclei is suggested by Lane [10, 11] and is expressed as

$$U(r) = U_{\rm o}(r) + 4\frac{\vec{t}\cdot\vec{T}}{A}U_1(r) + U_{\rm s.o.}(r) + \left(\tfrac{1}{2} - t_Z\right)V_{\rm C}(r)\,, \qquad (1)$$

where A is the mass of the nucleus, $U_{\rm s.o.}$ is the spin–orbit potential, and $V_{\rm C}$ is the Coulomb potential. The off-diagonal part of the potential U in the $\vec{t}\cdot\vec{T}$ space yields the quasielastic (p,n) transitions leading to the isobaric analog states. Since $\vec{t}$ and $\vec{T}$ are the isospins of the projectile and the target,

respectively, then the second term of Eq. (1) represents the isospin dependent $\vec{t}\cdot\vec{T}$ term. This term leads to terms t_+T_-, t_-T_+, and t_zT_z corresponding to the (p,n), (n,p), and (p,p) or (n,n) nuclear reaction processes, respectively. Therefore, while the diagonal part of U in the term $\vec{t}\cdot\vec{T}$ in Eq. (1) shows the influence of the isovector potential on elastic scattering, the off-diagonal t_+T_- part stands for the quasielastic (p,n) transition between the ground state and the associated isobaric analog state. Then, the quasielastic (p,n) scattering transition isovector potential is given by

$$U_{\rm qe}(r) = \left(2/A^{1/2}\right)\left\{\left[\rho_n(r)-\rho_p(r)\right]/\left[\rho_n(r)+\rho_p(r)\right]\right\}^{1/2} U_1(r)\,. \qquad (2)$$

In Eq. (2), the quasielastic scattering potential is using the asymmetry realistic nuclear densities calculated from effective density dependent force nucleon–nucleon interaction. The isovector component of the spin–orbit form factor together with the energy-dependent potential depth normalizations factors are used to obtain the spin–orbit part of the (p,n) transition potential. Since then, the isovector potential $U_1(r)$ can be given in the form of parametrized Woods–Saxon form

$$\begin{aligned} U_1(r,\rho,E) \;=\; & V_1(\rho,E)\left[1+e^{(r-r_{\rm R}(A))/a_{\rm R}(A)}\right]^{-1} \\ & -4ia_{\rm I}(A)W_1(\rho,E)\frac{d}{dr}\left[1+e^{(r-r_{\rm I}(A))/a_{\rm I}(A)}\right]^{-1}. \end{aligned} \qquad (3)$$

In Eq. (3), $V_1(\rho,E)$ and $W_1(\rho,E)$ represent the real and imaginary potentials, each including the corresponding isovector potentials. The nucleon–nucleus optical potential is density-dependent and obtained from the elastic nucleon scattering. Also, these energy-dependent nucleon–nucleus optical model potential depths are parametrized and normalized, for both of the isoscalar and isovector components. Then, the potential for the quasielastic (p,n) reactions leading to isobaric analog states is used in the distorted wave Born approximation to calculate both of the entrance and exit channels distorted waves.

3. Numerical calculations and results

Differential cross-sections of the quasielastic (p,n) reactions on different target nuclei and leading to isobaric analog states transitions are calculated using the distorted wave Born approximation. Optical model potentials are adjusted to deduce the proton and neutron scattering cross-sections. These optical potentials are used as first estimate for the isoscalar components in performing the distorted wave calculations of the quasielastic (p,n) scattering. The same can be done for the isovector components of the optical

model potential. Then, we reach the parametrized and normalized energy and density dependent potential depths. Therefore, the normalized isoscalar and isovector real and imaginary parts of the optical model potential representing the real and imaginary potential depths are given as

$$V_1(\rho,E) = \left(6.61+2.18A^{1/3}\right)\left[0.903+0.0007\ln(1000E)\right] \times\left[1.45-0.63\left(1+e^{(E-1.32)/3}\right)^{-1}\right] \tag{4}$$

and

$$W_1(\rho,E) = \left(5.12+0.36A^{1/3}\right)\left[1.17-\left(1+e^{(E-4.8)/3.5}\right)^{-1}\right] \times\left\{1.09+0.42\left[1+\left(e^{(E-38)/48.8}\right)^{4}\right]^{-1}\right\}. \tag{5}$$

The geometrical parameters of the nucleon–nucleus optical model potentials are also determined. The radius r_{R} and the diffuseness a_{R} parameters of the real part of the potential are taken to have the same values used previously [12] only for the purpose to reduce the number of parameters to be fitted. The radius of the imaginary part of the potential r_{I} and the diffuseness parameter a_{I} are then after searching given as

$$r_{\mathrm{I}} = 1.89-0.13A^{1/3} \tag{6}$$

and

$$a_{\mathrm{I}} = -0.083+0.21A^{1/3}\,. \tag{7}$$

The radial wave functions of the single particles in the distorted wave Born approximation calculations are obtained using Woods–Saxon potentials with radius $r_{\mathrm{o}} = 1.23$ fm, diffuseness $a = 0.58$ fm and $V_{\mathrm{l.s.}} = 5.8$ MeV, and the depth normalized to fit the valence nucleon binding energy.

The microscopic distorted-wave Born approximation calculations are used to compare the corresponding data by using the DWBA computer code. The calculations include also exchange effects such as knock-on effects which contribute to the cross-sections. The entrance channel parameters of the optical model are used as those of Becchetti and Greenless [12]. In the exit channel, self-consistent potential parameters are derived and used in the DWBA calculations. In the microscopic analysis, effective nucleon–nucleon interactions are used in the calculations.

Numerical calculations are carried out for the differential cross-sections of the quasielastic (p,n) reactions on different target nuclei. The calculations are performed for protons incident with different energies 23 MeV,

26 MeV and 35 MeV incident on the different target nuclei ^{13}C, ^{70}Zn, ^{96}Zr, ^{112}Sn, ^{124}Sn and ^{208}Pb. The geometrical parameters for the real part of the nucleon–nucleus potential are used to have the values taken by Becchetti and Greenless [12], while those for the imaginary part of the potential are obtained using Eqs (6),(7). These values are introduced with distorted wave Born approximation calculations to reproduce the differential cross-sections of the quasielastic (p, n) reactions leading to isobaric analog states transitions. The result of the calculated differential cross-sections are compared with the experimental data and previous calculations [2, 9]. The results of the present calculations are shown in figures 1–7 by the solid curves which better reproduce the experimental data.

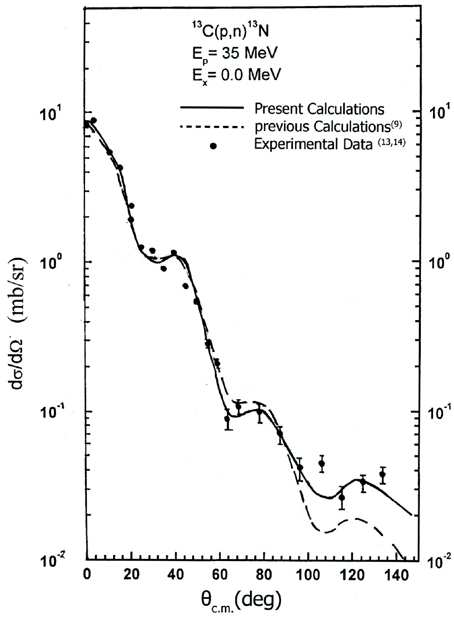

Fig. 1. Angular distribution for the ^{13}C$(p, n)^{13}$N reaction at incident proton energy E_p = 35 MeV leading to the ground state of ^{13}N. The dashed curve is the previous calculation [9]. The solid curve is our present calculation. The dots are the experimental data [13, 14].

4. Discussion and conclusions

In the present work, distorted wave Born approximations calculations are carried out for the differential cross-sections of the quasielastic (p, n) reactions leading to isobaric analog states transitions. The results of the present calculations of the angular distributions are in a good agreement with the experimental data as shown in figures 1–7. From the present analyses, the

real and imaginary isoscalar and isovector parts of the nucleon–nucleus optical model potential are energy-dependent, while the geometrical radius and diffuseness parameters are mass number dependent linearly with $A^{1/3}$. From figures 1–7, we see that the present theoretical calculations match the shapes as well as the amplitudes of the experimental data, where all of its essential features are very well described by the present calculations. The results of the calculated angular distributions are in a good agreement with experimental data, where the peaks are too large and too narrow especially at the forward scattering angles. Since the real and imaginary components of $U_1(r)$ exist only in the central part of the (p, n) transition potential given by Eq. (2), the quasielastic (p, n) scattering forms a good test for the isovector components of the optical model potential. We notice that the forward angle data are very well reproduced using the present optical model potential calculation, while the backward angle quasielastic scattering cross-sections are underestimated. It is expected to lower the backward angle differential cross-sections by considering the coupling of the analog-excited levels, which is not considered in the present calculations. The isobaric analog excitations are studied [19] microscopically following the folding model using phenomenological potentials, by introducing the isovector density dependence in the analysis.

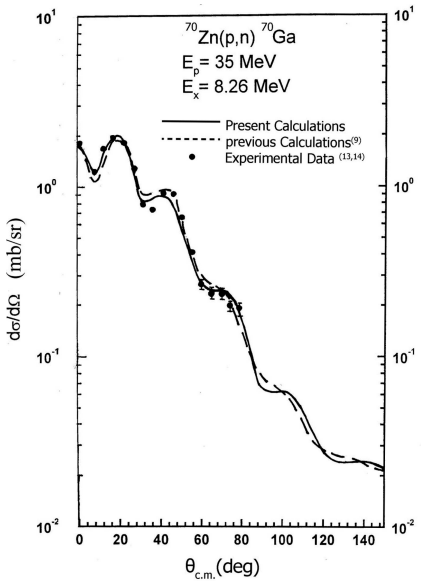

Fig. 2. Angular distribution for the ^{70}Zn$(p, n)^{70}$Ga reaction at incident proton energy $E_p = 35$ MeV leading to the 8.26 MeV isobaric analog state in ^{70}Ga. The dashed curve is the previous calculation [9]. The solid curve is our present calculations. The dots are the experimental data [13, 14].

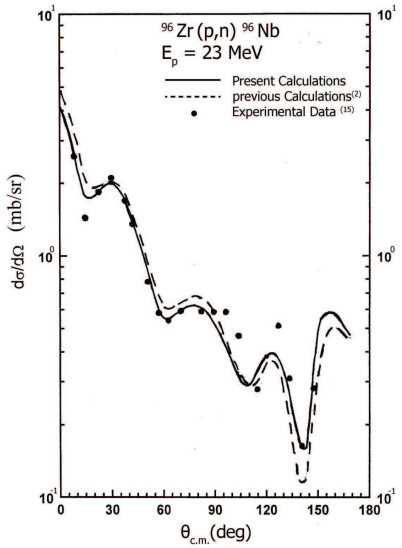

Fig. 3. Differential cross-sections of $^{96}\mathrm{Zn}(p,n)^{96}\mathrm{Nb}$ reaction at incident proton energy $E_p = 23$ MeV. The dashed curve is the previous calculation [2]. The solid curve is our present calculation. The dots are the experimental data [15].

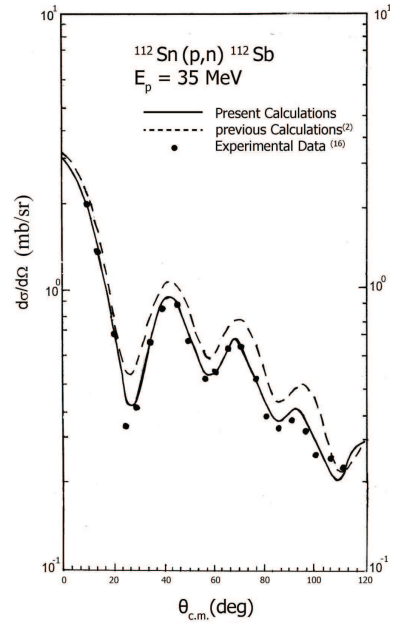

Fig. 4. Differential cross-sections of the $^{112}\mathrm{Sn}(p,n)^{112}\mathrm{Sb}$ reaction at incident proton energy $E_p = 35$ MeV. The dashed curve is the previous calculation [2]. The solid curve is our present calculation. The dots are the experimental data [16].

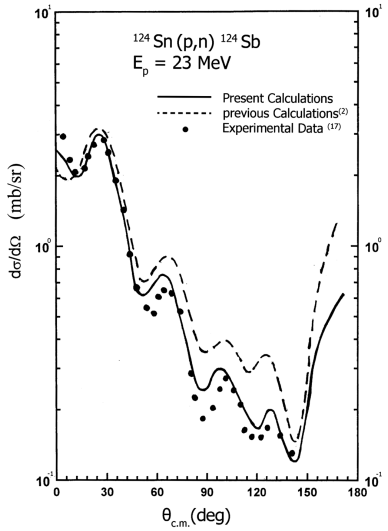

Fig. 5. Differential cross-sections of the $^{124}\mathrm{Sn}(p,n)^{124}\mathrm{Sb}$ reaction at incident proton energy $E_p = 23$ MeV. The dashed curve is the previous calculation [2]. The solid curve is our present calculation. The dots are the experimental data [17].

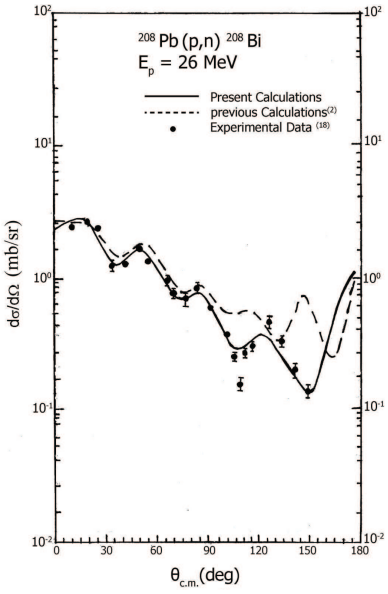

Fig. 6. Differential cross-sections of the $^{208}\mathrm{Pb}(p,n)^{208}\mathrm{Bi}$ reaction at incident proton energy $E_p = 26$ MeV. The dashed curve is the previous calculation. The solid curve is our present calculation. The dots are the experimental data [18].

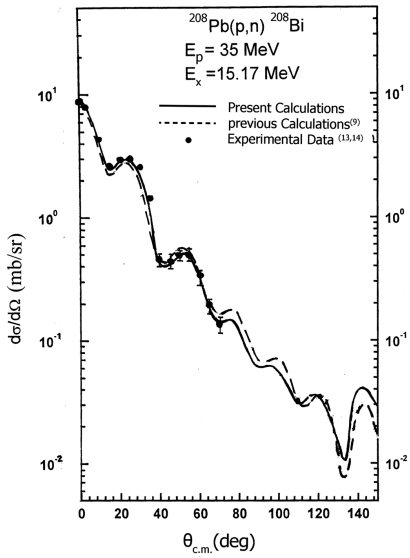

Fig. 7. Angular distribution for the $^{208}\mathrm{Pb}(p, n)^{208}\mathrm{Bi}$ reactions at incident proton energy $E_p = 35$ MeV leading to the 15.17 MeV isobaric analog state in ^{208}Bi. The dashed curve is the previous calculation [9]. The solid curve is our present calculation. The dots are the experimental data [13, 14].

The obtained present results are in a good agreement with the experimental data [13–18]. The present calculations of the differential cross-sections show the oscillatory pattern, and fit the position of the peaks. Also, the present calculations extract larger values for the angular distributions at backward angles, with better and good agreement with the data.

The nucleon–nucleus optical model potentials for the quasielastic (p, n) reactions leading to isobaric analog states transitions depend on the potential depths and on the local asymmetry parameter $\alpha(r)$, where $\alpha(r) = [\rho_n(r) - \rho_p(r)]/[\rho_n(r) + \rho_p(r)]$, dealing with finite nuclei improved local density approximation. The good agreement between the present theoretical calculations and measured data shows the importance of the isovector components of the nucleon–nucleus optical model potential.

Therefore, we can conclude that the energy density as well as the energy-dependence of the real and imaginary parts of the isoscalar and isovector components of the nucleon–nucleus optical model potentials are very important and should be included in calculating the differential cross-sections of the quasielastic (p, n) reactions leading to isobaric analog states transitions.

REFERENCES

[1] D.T. Koa, G.R. Satchler, *Nucl. Phys.* **A668**, 3 (2000).
[2] E. Bauge, J.P. Delaroche, M. Girod *Phys. Rev.* **C63**, 024607 (2001).
[3] F. Maréchel *et al.*, *Phys. Rev.* **C60**, 034615 (1999).
[4] W. Zuo, I. Bombaci, U. Lombardo, *Phys. Rev.* **C60**, 024605 (1999).
[5] G. Colò, N. van Giai, *Phys. Rev.* **C53**, 2201 (1996).
[6] T. Suzaki, H. Sagawa, G. Colò, *Phys. Rev.* **C54**, 2954 (1996).
[7] U. Van Kolck, J.L. Friar, T. Goldman, *Phys. Lett.* **B271**, 169 (1996).
[8] H. Orihara *et al.*, *Phys. Lett.* **81**, 3607 (1998).
[9] G.C. Jon *et al.*, *Phys. Rev.* **C62**, 044609 (2000).
[10] A.M. Lane, *Nucl. Phys.* **35**, 676 (1962).
[11] A.M. Lane, *Phys. Rev.* **8**, 171 (1962).
[12] F.D. Becchetti, G.W. Greenless, *Phys. Rev.* **182**, 1190 (1969).
[13] H. Orihara, T. Murakami, *Nucl. Instrum. Methods* **181**, 15 (1981).
[14] H. Orihara *et al.*, *Nucl. Instrum. Methods Phys. Res.* **A257**, 189 (1987).
[15] J. Gosset, B. Mayer, J.L. Escudié, *Phys. Rev.* **C14**, 878 (1974).
[16] S.D. Schery *et al.*, *Phys. Lett.* **79B**, 30 (1978).
[17] S.D. Schery, D.A. Lind, H. Wieman, *Phys. Rev.* **C14**, 1800 (1976).
[18] S.D. Schery, D.A. Lind, H.W. Fielding, C.D. Zafiratos, *Nucl. Phys.* **A234**, 109 (1974).
[19] D.T. Khoa, H.S. Than, D.C. Cuong, *Phys. Rev.* **C76**, 014603 (2007).